Phase transitions of anisotropic and exchange origins in $TmFe_5Al_7$

D. I. Gorbunov,[1,2,*] S. Yasin,[3] A. V. Andreev,[1] N. V. Mushnikov,[4] E. V. Rosenfeld,[4] Y. Skourski,[3] S. Zherlitsyn,[3] and J. Wosnitza[3,5]

[1]*Institute of Physics, Academy of Sciences, Na Slovance 2, 182 21 Prague, Czech Republic*

[2]*Department of Condensed Matter Physics, Charles University, Ke Karlovu 5, 121 16 Prague, Czech Republic*

[3]*Dresden High Magnetic Field Laboratory (HLD), Helmholtz-Zentrum Dresden-Rossendorf, D-01314 Dresden, Germany*

[4]*Institute of Metal Physics, Ural Branch of Russian Academy of Sciences, Kovalevskaya 18, 620990 Ekaterinburg, Russia*

[5]*Institut für Festkörperphysik, TU Dresden, D-01062 Dresden, Germany*

(Received 21 March 2014; revised manuscript received 15 May 2014; published 20 June 2014)

Magnetization and sound propagation reveal a number of unusual spontaneous and field-induced transformations in ferrimagnetic $TmFe_5Al_7$ ($T_C = 193$ K). The rare-earth sublattice was found to provide a uniaxial magnetic anisotropy, whereas the iron sublattice favors an easy-plane anisotropy. A competition between them results in a first-order spin-reorientation transition at 64 K as the magnetic moments rotate from the c axis to the basal plane of a tetragonal structure. The transition is preceded by a first-order magnetization process of type II along the hard axis. Remarkably, the intersublattice Tm-Fe exchange interaction is weakened at the spin-reorientation transition. Concomitantly, the spontaneous magnetic moment disappears, and the ferrimagnetic state changes to antiferromagnetic. With increasing temperature, the strength of the Tm-Fe exchange is recovered, and the ferrimagnetism is restored at 82 K through another first-order phase transformation. Below 40 K, a first-order field-induced transition occurs for a magnetic field applied along the easy [001] axis. It reflects a rotation of the magnetic moments towards the forced ferromagnetic state observed above 30 T. Along the hard [100] axis the ferromagnetic saturation is not reached even at 60 T.

DOI: 10.1103/PhysRevB.89.214417 PACS number(s): 75.30.Kz, 75.50.Gg, 75.30.Gw, 62.65.+k

I. INTRODUCTION

In $3d$-$4f$ intermetallic compounds, the magnetic anisotropy originates in two separate contributions associated with the transition-metal sublattice and the rare-earth sublattice (see, for example, Refs. [1] and [2]). At low temperatures, the main anisotropy usually is provided by the rare-earth sublattice [3–12]. The magnetocrystalline anisotropy of the rare-earth sublattice is single ion in nature, that is, it originates from the electrostatic interaction between the crystal electric field and the aspherical $4f$-electron-charge cloud (the coupling between the orbital and spin moment of the $4f$ orbital proceeds via spin orbit interaction). In first approximation, the shape of the $4f$ orbital is described by the second-order Stevens factor, α_J, of the R^{3+} ion. In the same crystal electric field, a change of the shape of the $4f$ orbital from an oblate ($\alpha_J < 0$) to a prolate ($\alpha_J > 0$) spheroid normally leads to a change of magnetocrystalline anisotropy.

Rare-earth $3d$ transition-metal compounds crystallizing in the tetragonal $ThMn_{12}$-type structure are not only interesting in view of their potential application as permanent magnets (see for review Ref. [13]) but also from a more fundamental perspective. Depending on the content of $3d$ metal, some of these materials exhibit a strong magnetic hysteresis and other unusual effects. For instance, a "negative magnetization" (antiparallel orientation between the sample's total magnetization and the external magnetic field) was observed in polycrystalline samples of the ferrimagnets RFe_5Al_7 (R = Tb, Dy, Ho, and Er) [14,15].

The crystal structure of RFe_5Al_7 compounds is rather simple (space group $I4/mmm$; see Fig. 1): the R atoms reside on the $2a$ site, Fe and Al completely occupy the $8f$ and $8i$ sites, respectively, and share the $8j$ site.

The RFe_5Al_7 compounds, with R = Tb, Dy, Ho, Er, and Tm, are collinear ferrimagnets [16]. Detailed systematic studies performed on RFe_5Al_7 single crystals, with R = Tb, Dy, Ho, and Er confirmed the high magnetic anisotropy [17–20]. Curiously, it was found that the crystal-field-induced anisotropy of the rare-earth sublattice is not modified as the sign of the second-order Stevens factor α_J of the R^{3+} ion changes. No competition was observed between the anisotropies of the rare-earth and iron sublattices, although $\alpha_J < 0$ for Tb, Dy, and Ho, but $\alpha_J > 0$ for Er [2]. The Fe sublattice displays an easy-plane anisotropy [21–23]; therefore, the rare-earth sublattices contribute to the magnetic anisotropy in the same way. The apparent controversy for $ErFe_5Al_7$ is most likely due to a small α_J value for Er, as a result of which the dominant negative contribution to the anisotropy of the Er sublattice is given by its higher order terms (fourth- and sixth-order terms) [19]. A similar situation was found in the isostructural compounds $ErFe_{11}Ti$, $ErFe_{10}Mo_2$, and $ErFe_{10.5}V_{1.5}$, where the Er sublattice does not exhibit a uniaxial magnetic anisotropy [24–26], contrary to the expectations.

A way to change the magnetic anisotropy of the rare-earth sublattice in RFe_5Al_7 is to use Tm as a rare-earth component. For Tm^{3+}, the second-order Stevens factor is positive and much larger than for Er^{3+} [2]. For this reason, the single-ion magnetocrystalline anisotropy of the Tm sublattice is expected to be uniaxial. The compound should display easy-axis anisotropy (preferable moment orientation is along the tetragonal axis) at low temperatures where the relative Tm contribution is strongest. A competition between the uniaxial Tm and multiaxial Fe magnetic anisotropies should occur, leading to a spontaneous spin-reorientation transition.

The magnetic anisotropy also plays an important role in determining the behavior of ferrimagnetically ordered

*Corresponding author: gorbunov@fzu.cz

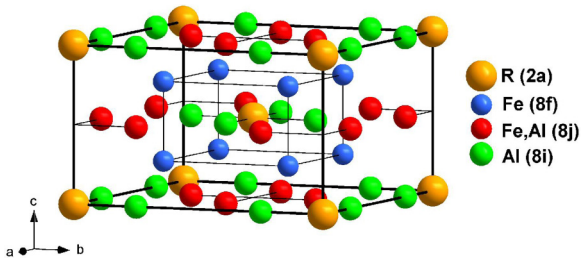

FIG. 1. (Color online) Crystal structure of RFe_5Al_7.

compounds in a magnetic field. One can expect that the application of a sufficiently strong field leads to a rotation of the magnetic moments from the initial ferrimagnetic structure through a canted structure to the final collinear ferromagnetic state. In the simplest case of an isotropic ferrimagnet, the Zeeman energy competes against the intersublattice exchange energy. In these conditions, the ferrimagnetic saturation is followed by a canting of the intersublattice moments towards the field direction until the forced ferromagnetic state is reached [27]. The magnetic anisotropy in real materials results in a more complex magnetization process [28]. Magnetic moments may show stepwise rotation along certain crystallographic directions in an applied field.

A number of field-induced magnetic phase transitions have indeed been found in the highly anisotropic ferrimagnets RFe_5Al_7, with R = Tb, Dy, Ho, and Er [17–20,29–32]. Simultaneous stepwise rotations of the R and Fe magnetic moments occur along high-symmetry crystallographic directions in the basal plane. Field-induced magnetic transitions are likely to occur in $TmFe_5Al_7$ in an applied magnetic field because it is also ferrimagnetic. In this sense, $TmFe_5Al_7$ is a particularly interesting system since its easy magnetization direction (EMD) is expected to be out of the basal plane, leading to a different magnetic symmetry and, therefore, different field-induced rotations of the magnetic moments. The occurrence of field-induced anomalies has been reported in the uniaxial ferrimagnets based on Tm and 3d-metals, Tm_2Co_{17} [33] and Tm_2Fe_{17} [34], having a hexagonal crystal lattice of Th_2Ni_{17} type. Rather unusual transitions were observed: the transition into the forced ferromagnetic state occurs in Tm_2Co_{17} through a continuous remagnetization of the Tm sublattice, whereas Tm_2Fe_{17} displays four consecutive metamagnetic transitions at which the magnetization increases in steps whose heights correspond to the Tm magnetic moment, 7 μ_B.

Here, we present a study of the spontaneous and field-induced magnetic phase transitions in $TmFe_5Al_7$ through an investigation of the magnetic and magnetoelastic properties. So far, no detailed information was available on the magnetocrystalline anisotropy of $TmFe_5Al_7$. We measured the magnetization and the relative changes of the sound velocity and sound attenuation in static (up to 18 T) and pulsed (up to 60 T) magnetic fields along the principal crystallographic directions of a single crystal.

II. EXPERIMENTAL DETAILS

A $TmFe_5Al_7$ single crystal was grown by a modified Czochralski method in a triarc furnace from a stoichiometric mixture of the pure elements (99.9% Tm, 99.98% Fe, and 99.999% Al). The crystal structure was determined using standard powder x-ray diffraction performed on a part of the single crystal crushed into fine powder. The obtained lattice parameters of the tetragonal unit cell, a = 865.8 pm and c = 503.2 pm, are in good agreement with those obtained in Ref. [14] on a polycrystalline sample. Backscattered Laue patterns were used to confirm the single-crystalline state and to orient the crystal to cut samples for magnetization, specific heat, and acoustic measurements.

The field dependence of the magnetization between 2 and 280 K was measured along the principal crystallographic directions [100], [110], and [001] using a standard Physical Property Measurement System (PPMS)-14 magnetometer (Quantum Design) in static magnetic fields up to 14 T. All magnetization curves are presented as a function of the internal magnetic field intensity $\mu_0 H_i$. The specific heat was measured by use of the relaxation method in the PPMS between 2 and 300 K in zero magnetic field.

The magnetization in pulsed magnetic fields up to 60 T (pulse duration 20 ms) was measured between 2 and 80 K at Dresden High Magnetic Field Laboratory. The experimental setup was described in detail in Ref. [35]. Absolute values of the magnetization were calibrated using data from measurements in static magnetic field.

Relative changes of the ultrasound velocity and sound attenuation were measured using a pulse-echo technique [36,37] in steady fields up to 18 T between 2 and 240 K and in pulsed fields up to 60 T between 2 and 40 K. Two piezoelectric film transducers were glued to opposite surfaces of the single crystal in order to excite and detect acoustic waves. The longitudinal acoustic wave propagated with a wave vector $\boldsymbol{k}$ and polarization $\boldsymbol{u}$ along the [001] axis of the single crystal. The field $\boldsymbol{H}$ was applied along the [001] axis as well. Transverse ultrasound waves ($\boldsymbol{k}$ and $\boldsymbol{H}$ are parallel to the [001] axis, $\boldsymbol{u}$ is parallel to the [110] axis) have also been utilized but yielded much weaker anomalies at the spontaneous and field-induced phase transitions.

III. RESULTS AND DISCUSSION

Figure 2 shows the magnetization measured at 2 and 120 K for fields up to 8 T applied along the [100] and [001]

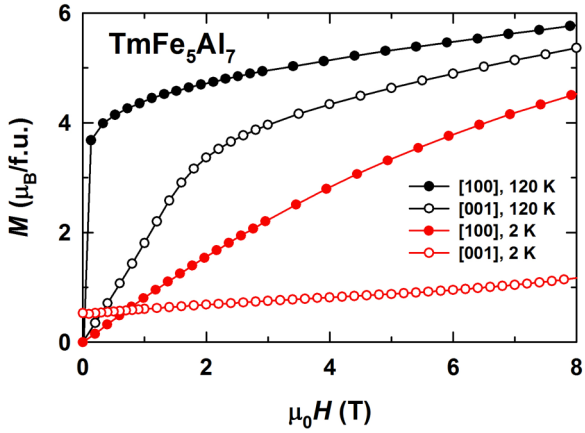

FIG. 2. (Color online) Magnetization curves along the [100] and [001] axes of $TmFe_5Al_7$ at 2 and 120 K.

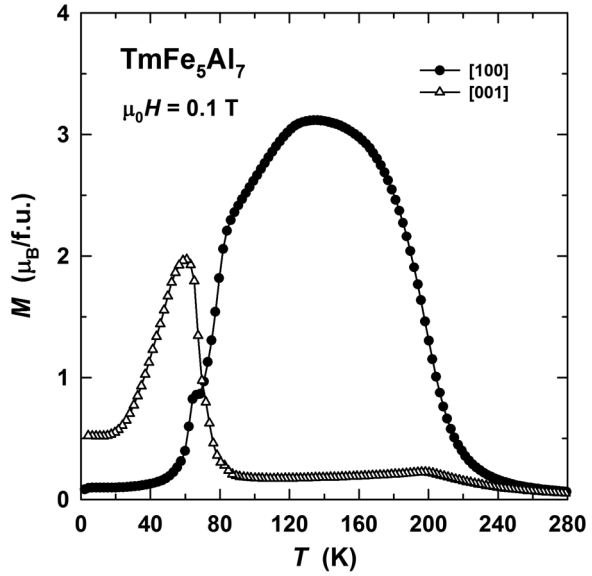

FIG. 3. Temperature dependence of the magnetization for a field of 0.1 T applied along the [100] and [001] axes.

axes of $TmFe_5Al_7$. At $T = 2$ K, the EMD is along the c axis with a spontaneous magnetic moment of $M_s = 0.5\ \mu_B$/f.u. In the whole temperature range of the ferrimagnetic state, the magnetic moment of the Fe sublattice is higher than that of the Tm sublattice. Therefore, there is no compensation point in $TmFe_5Al_7$ (see Fig. 3 below), in contrast to the compounds with $R =$ Tb, Dy, Ho, and Er [17–20]. An intensive increase in the magnetization along the hard axis leads to an intersection of the magnetization curves at 2 K. This is a result of a field-induced noncollinearity of the sublattice moments due to a relatively weak Tm-Fe intersublattice exchange. No anomalies are observed at the intersection point. Assuming that at 2 K the Tm magnetic moment is equal to that of a free Tm^{3+} ion, 7 μ_B, and that the compound is a collinear ferrimagnet, the magnetic moment of the Fe sublattice can be calculated as follows: $M_{Fe} = M_s + M_{Tm} = 7.5\ \mu_B$/f.u. This corresponds to 1.5 μ_B per Fe atom, a typical value for RFe_5Al_7 compounds [17–23]. Magnetization curves were also measured for fields applied along the [110] axis, showing no difference to the data for $\boldsymbol{H} \| [100]$. This reflects a negligible anisotropy within the basal plane at all temperatures, whereas this anisotropy is large in other RFe_5Al_7 compounds with magnetic R [17–21,23]. Figure 2 also shows that at 120 K the EMD is along the [100] axis, in contrast to the situation at 2 K. Therefore, a spin-reorientation transition occurs in $TmFe_5Al_7$ from the [001] axis to the (001) plane with increasing temperature.

Figure 3 shows the temperature dependence of the magnetization for a field of 0.1 T applied along the [100] and [001] axes of $TmFe_5Al_7$. Growing from low temperatures, the magnetization for $\boldsymbol{H} \| c$ (the EMD) shows a pronounced maximum at about 60 K, then at about 70 K the magnetization reduces drastically and the spin-reorientation transition occurs. With increasing temperature, the magnetization falls off in the vicinity of 200 K as the compound becomes paramagnetic.

In the specific heat, two anomalies at 63 and 72 K appear, as shown in Fig. 4(a). In the sound velocity of a longitudinal acoustic mode as well an anomaly appears around 63 K

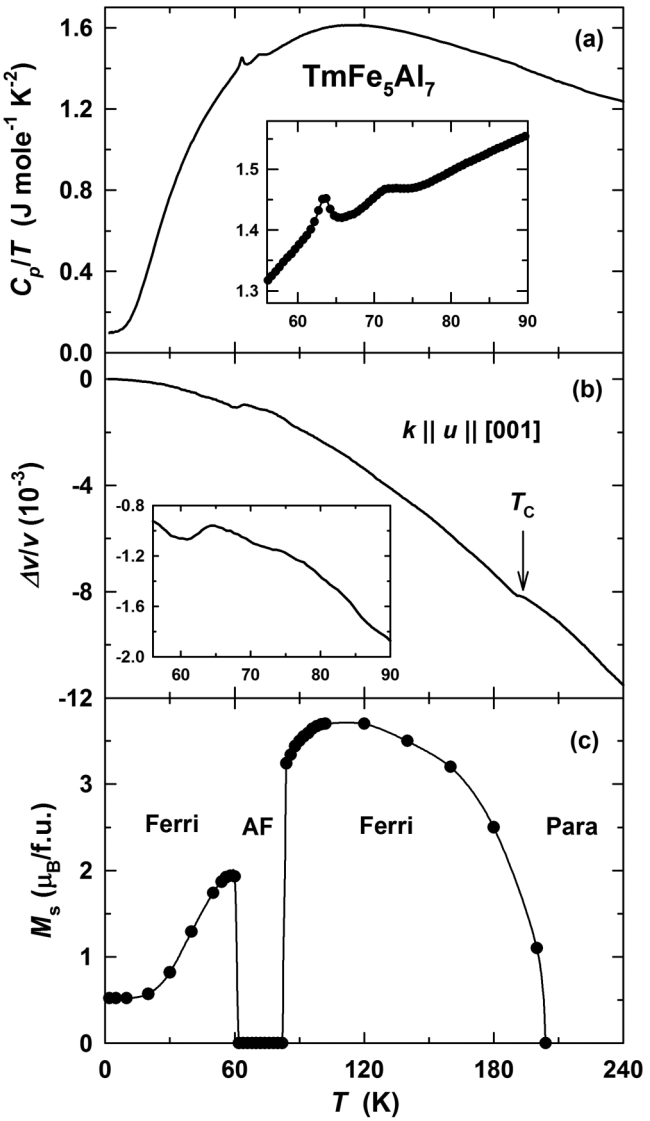

FIG. 4. Temperature dependence of (a) the specific heat plotted as C_p/T; (b) the relative sound-velocity change, $\Delta v/v$, of a longitudinal acoustic wave propagating along the [001] axis; and (c) the spontaneous magnetic moment, M_s, of $TmFe_5Al_7$. The insets in the upper and middle panels show C_p/T and $\Delta v/v$, respectively, in the vicinity of the spin-reorientation transition. The ferrimagnetic state is denoted by Ferri, antiferromagnetic by AF and paramagnetic by Para.

[Fig. 4(b)]. In addition, a weak feature is seen in $\Delta v/v$ at 193 K (shown by arrow), which is related to the phase transition into the paramagnetic state; however, the spontaneous magnetic moment drops to zero only slightly above 200 K [Fig. 4(c)]. A small applied magnetic field induces a small moment even above T_C, and a standard Arrott-plot treatment does not provide a proper T_C value. For this reason, T_C can be determined accurately only in zero field. In the specific heat, no feature can be resolved in the vicinity of 200 K, which means that the ferrimagnetic phase transition results in a rather small entropy change. In order to elucidate the origin of the anomalies in C_p/T and $\Delta v/v$ around 60–70 K, we analyzed the magnetization curves within this temperature interval.

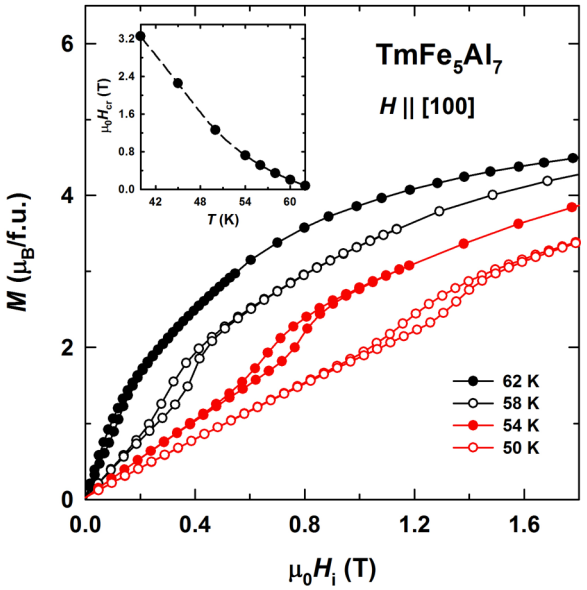

FIG. 5. (Color online) Magnetization as a function of field applied along the [100] axis of $TmFe_5Al_7$ between 50 and 62 K. The inset shows the temperature dependence of the FOMP critical field.

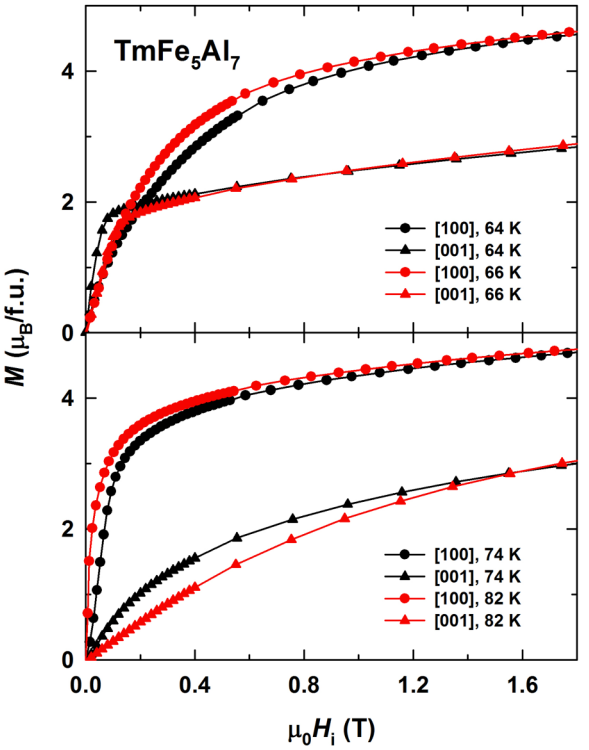

FIG. 6. (Color online) Magnetization as a function of field applied along the [100] and [001] axes of $TmFe_5Al_7$ between 64 and 82 K.

For fields applied along the hard [100] axis, S-shaped magnetization curves are found in the temperature range between 50 and 62 K (Fig. 5). The observed field-induced magnetic transition is a first-order magnetization process (FOMP). This is a so-called type-II FOMP because the magnetization immediately after the transition does not reach the easy-axis value but continues to grow. The FOMP is observed in the temperature range between 40 and 62 K. Below 40 K, no magnetization jump is seen along the hard [100] axis in the field range where the FOMP is likely to occur. (A magnetization jump is observed at a much higher field, ≈37 T; however, that has a different origin, see below.) This is unexpected since with decreasing temperature the field-induced transition should not disappear but rather become more pronounced. The FOMP is of anisotropic nature, therefore, the observed changes reflect a rather intricate balance between anisotropy constants involved in the process. The FOMP critical field determined as the average field between the ascending and descending branches decreases monotonously with temperature (inset in Fig. 5). One would assume that as soon as the FOMP disappears, that is, when its critical field reaches zero, a spontaneous magnetic moment should appear for $\boldsymbol{H}\|[100]$ axis (just above 62 K). However, this is not observed in the experiment.

At 64 K, $TmFe_5Al_7$ displays no spontaneous magnetic moment for fields applied along the [100] and [001] axes (Fig. 6). At low fields, the magnetization is still larger for $\boldsymbol{H}\|[001]$. At 66 K, the compound is practically isotropic in the low-field region. With increasing temperature, the slope of the magnetization curve for $\boldsymbol{H}\|[100]$ becomes gradually more vertical. Nevertheless, no spontaneous magnetic moment is observed up to 82 K.

Low-field details of the magnetization for $\boldsymbol{H}\|[100]$ between 70 and 86 K are shown in Fig. 7. Below 74 K, the magnetization is a featureless function of field. At 74 K, a hysteretic magnetization jump develops. This is obviously not a domain hysteresis; the sample's coercivity is very small. With increasing temperature, the jump and its hysteresis become more pronounced. At 86 K, the jump disappears and a spontaneous magnetic moment appears. Moreover, a typical hysteresis caused by ferrimagnetic domains is observed. Above 82 K, a nonzero spontaneous magnetic moment exists along the easy [100] axis with increasing temperature.

The temperature dependence of the spontaneous magnetic moment, M_s, of $TmFe_5Al_7$ in the whole magnetically ordered state is shown in Fig. 4(c). M_s follows the temperature dependence of the magnetization for $\boldsymbol{H}\|[001]$ below 64 K and for $\boldsymbol{H}\|[100]$ above 82 K. Between 64 and 82 K the spontaneous magnetic moment is zero along both, [100] and [001], axes.

Based on the results presented, we propose the following interpretation of the magnetic behavior of $TmFe_5Al_7$. In accordance with the specific heat and sound-velocity measurements, a phase transition occurs at 64 K when the magnetic moments rotate from the c axis to the basal plane (schematic moment configurations are given in Fig. 8). This is likely a first-order transition since no intermediate easy cone phase was observed. Simultaneously, the spontaneous magnetic moment disappears, with M_s being zero up to 82 K. The absence of a spontaneous magnetic moment can be related either to a paramagnetic or an antiferromagnetic state. The former is not possible since between 82 K and T_C a spontaneous magnetic moment exists and the compound displays a usual ferrimagnetic behavior. Therefore, the absence of a spontaneous magnetic moment in $TmFe_5Al_7$ between 64 and 82 K is related to an antiferromagnetic

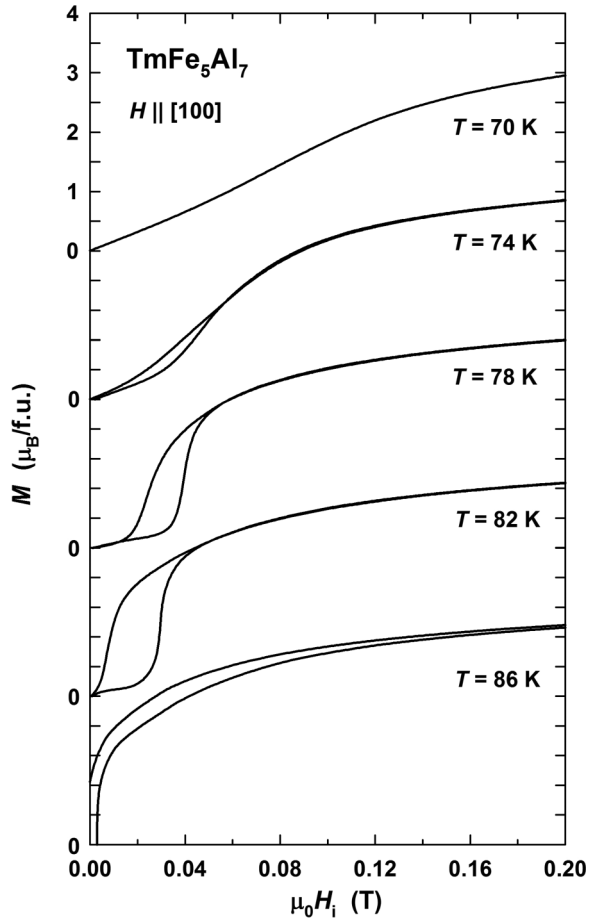

FIG. 7. Low-field details of the magnetization for fields applied along [100] between 70 and 86 K.

spin arrangement [Fig. 8(b)]. Around 84 K, the antiferromagnetic structure changes back to ferrimagnetic [Fig. 8(c)]. In our opinion, the antiferromagnetic-ferrimagnetic phase transition is also of first order since it occurs when the hysteretic field-induced magnetization jump in the antiferromagnetic state comes to zero field (see Fig. 7). Such a set of unusual magnetic transitions may be due to a relatively weak exchange interaction between the Tm and Fe sublattices.

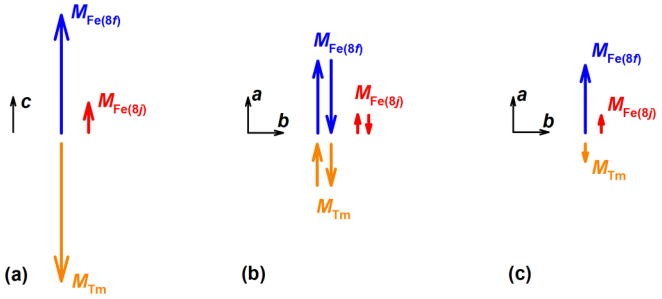

FIG. 8. (Color online) Schematic drawings of the zero-field moment configurations for the uniaxial ferrimagnetic (a), planar antiferromagnetic (b), and planar ferrimagnetic (c) states of $TmFe_5Al_7$.

An estimate of the intersublattice exchange constant, n_{TmFe}, in $TmFe_5Al_7$ can be made using molecular field theory. The Tm^{3+} ions are assumed to experience the mean molecular field $\mu_0 H_{mol} = n_{TmFe} \times M_{Fe}$ created by the Fe magnetic sublattice. It is this sublattice that provides the strongest exchange interactions in RFe_5Al_7 [17–23]. Therefore, the temperature dependence of the Tm magnetic moment is mainly determined by the Tm-Fe exchange interaction. The temperature dependence of M_{Tm} is obtained via the relation $M_{Tm}(T) = M_{Fe}(T) - M_s(T)$. The temperature dependence of the Fe magnetic moment, M_{Fe}, might be estimated using $LuFe_5Al_7$ as a reference compound; however, $LuFe_5Al_7$ has a complicated magnetic structure: antiferromagnetic exchange interactions are realized at low and ferromagnetic interactions at high temperatures [22]. For this reason, $M_{Fe}(T)$ of the isostructural collinear ferromagnet $LuFe_6Al_6$ [22,38] was used for the calculations by reducing $M_{Fe}(T)$ to T_C and M_{Fe} of $TmFe_5Al_7$ at $T = 2$ K. $M_{Tm}(T)$ thus determined was fitted by the Brillouin function, B_J, using the aforementioned molecular field H_{mol}:

$$M_{Tm}(T) = M_{Tm}(0)\, B_J\left(\frac{\mu_B J g \mu_0 H_{mol}}{k_B T}\right), \qquad (1)$$

where J and g are the quantum number of the total Tm moment and the Landé factor, respectively. Unfortunately, the agreement between the experimental and fitting curves is very poor for a wide range of $\mu_0 H_{mol}$ values. The reason might be a large error in the estimated $M_{Fe}(T)$. Moreover, between 64 and 82 K, the spontaneous magnetic moment of $TmFe_5Al_7$ is zero, and the Tm magnetic moment cannot be determined by magnetization measurements. Interestingly, the temperature dependence of the rare-earth magnetic moment can be determined rather precisely using molecular field theory for the isostructural compounds with $R =$ Tb, Dy, Ho, and Er [17,30–32]. $TmFe_5Al_7$ presents a more complicated case. A more thorough approach is necessary in order to calculate H_{mol}, e.g., the needed information on the crystal electric field could be obtained by inelastic neutron scattering.

The molecular field H_{mol} was found to vary linearly with spin, S, of the rare-earth component in the RFe_5Al_7 series (Fig. 9). Therefore, in order to estimate H_{mol} in $TmFe_5Al_7$, a linear extrapolation was made to $S = 1$ as relevant for $R =$ Tm. The obtained value is $\mu_0 H_{mol} = 16$ T (at 2 K), which corresponds to $n_{TmFe} = 2.1$ T f.u./μ_B. Using this value of the molecular field, an approximate temperature dependence of the Tm magnetic moment was calculated using Eq. (1). Due to the relatively weak Tm-Fe exchange interaction, M_{Tm} decreases much more rapidly at low temperatures than the magnetic moment of the Dy sublattice in isostructural $DyFe_5Al_7$ (inset in Fig. 9). Under these circumstances, the magnetic moment of the Fe sublattice should also decrease more rapidly than, e.g., M_{Fe} of RFe_5Al_7 with other magnetic heavy rare-earth elements and of $LuFe_6Al_6$ [17,30–32,38].

A change of the magnetic ordering within the Fe sublattice is likely to be the driving force behind the ferrimagnetic-antiferromagnetic transition in $TmFe_5Al_7$. In the crystal structure of RFe_5Al_7, the R atoms are located within the planes filled by Fe and Al atoms ($8j$ site). Just above and just below them at equal distances, there are planes of the $8f$ sites occupied exclusively by Fe atoms. Competitive exchange

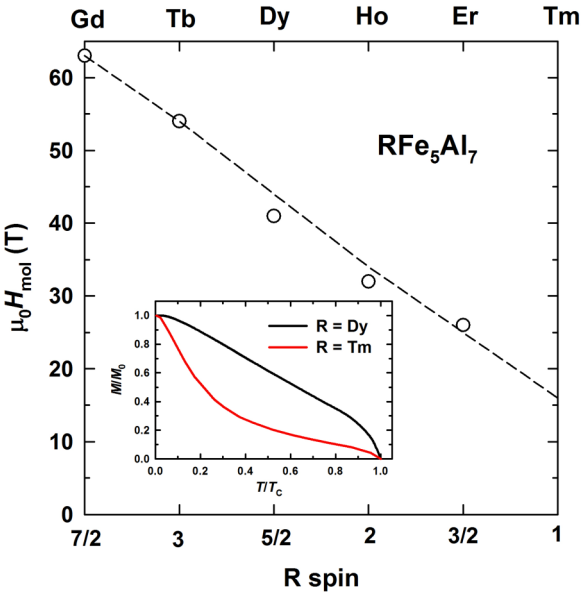

FIG. 9. (Color online) Dependence of the molecular field produced by the Fe sublattice on the rare-earth spin in $R\mathrm{Fe}_5\mathrm{Al}_7$ with $R =$ Gd, Tb, Dy, Ho, and Er (data from Refs. [21] and [29–32]). The inset shows the temperature dependence of the specific magnetization of the Dy and Tm sublattices in $\mathrm{RFe}_5\mathrm{Al}_7$.

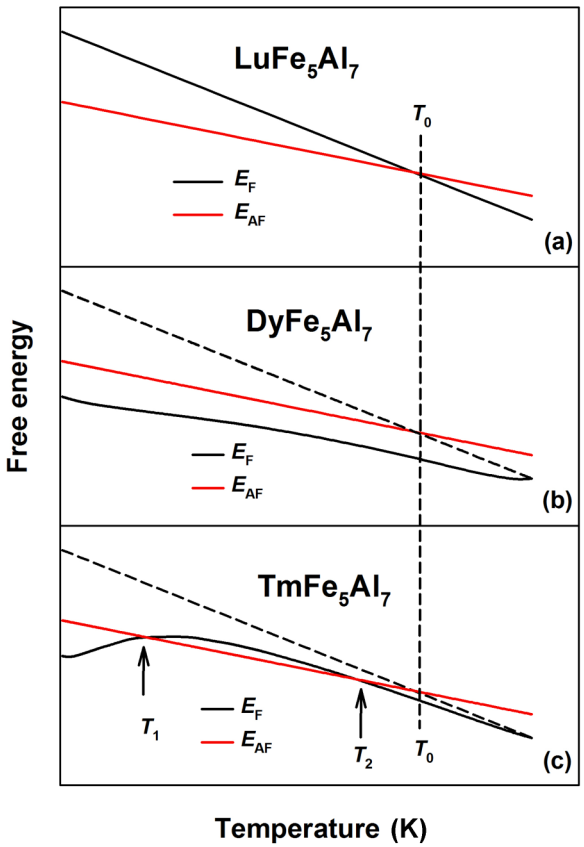

FIG. 10. (Color online) Schematic temperature dependence of the free energy of the ferromagnetic (F) and antiferromagnetic (AF) phases within the Fe sublattice of $\mathrm{RFe}_5\mathrm{Al}_7$ with R = Lu (a), Dy (b), and Tm (c).

interactions were reported for $\mathrm{LuFe}_x\mathrm{Al}_{12-x}$ compounds with nonmagnetic Lu [22]. It is reasonable to assume that within the Fe sublattice there are two types of Fe-Fe exchange interactions. Within the upper and lower planes of the $8f$ site, a ferromagnetic exchange interaction is stabilized. There is also an interplanar Fe-Fe exchange interaction that proceeds through the Fe atoms located in the planes filled by Fe and Al atoms. The sign and strength of the interplanar interaction depends on the Fe content. In the absence of a magnetic rare-earth component, with increasing temperature the transition from antiferromagnetic to ferromagnetic order appears in $\mathrm{LuFe}_5\mathrm{Al}_7$ around $T_0 = 80$ K [22]. Therefore, the free energies of the ferromagnetic, E_F, and antiferromagnetic, E_AF, phases in $\mathrm{LuFe}_5\mathrm{Al}_7$ become equal at T_0 as schematically shown in Fig. 10(a).

When R is a magnetic heavy rare-earth component, the negative R-Fe exchange interaction is stabilized, which strengthens the indirect positive Fe-R-Fe interplanar exchange interaction whose energy is roughly proportional to the average R magnetic moment (inset in Fig. 9). When the R-Fe exchange interaction is strong, as in, e.g., $\mathrm{DyFe}_5\mathrm{Al}_7$, the ferromagnetic phase is stable within the Fe sublattice in the whole temperature range of the magnetically ordered state [Fig. 10(b)]. When the R-Fe exchange interaction is weak, the ferromagnetic phase can only be stabilized at sufficiently low temperatures $T < T_1$. In the temperature range $T_1 < T < T_2$, the negative interplanar Fe-Fe exchange interaction results in the formation of an antiferromagnetic order. Finally, at T_2, slightly lower than T_0 (due to the influence of a small positive Fe-R-Fe interaction), the ferromagnetic state is again stabilized [Fig. 10(c)].

The spin-reorientation transition in $\mathrm{TmFe}_5\mathrm{Al}_7$ favors the disappearance of the spontaneous magnetic moment in a limited temperature range. Indeed, the spin reorientation is a result of the competition between the Tm and Fe anisotropies. Due to the weak Tm-Fe exchange interaction, this leads to the formation of a noncollinear magnetic structure in the vicinity of the transition: the Tm moment still sticks to the [001] axis, while the Fe moment tends towards the basal plane. Furthermore, the absolute value of the R moment decreases due to its rotation towards the hard magnetization direction. This effect was observed by use of neutron diffraction in $R\mathrm{Co}_5$ compounds at the spin-reorientation transitions [39]. The noncollinearity and reduced absolute value of the Tm magnetic moment weaken the Tm-Fe exchange interaction and facilitate the formation of the antiferromagnetic structure of the Fe magnetic moments within the basal plane.

Using this model, the unusual shape of the magnetization curves between 74 and 82 K can be easily explained (Fig. 7). The application of a magnetic field along the [100] axis induces a metamagnetic antiferromagnetic-ferromagnetic transition within the Fe sublattice. The Tm-Fe exchange interaction is strengthened, and the ferrimagnetic order in $\mathrm{TmFe}_5\mathrm{Al}_7$ is favored.

$\mathrm{TmFe}_5\mathrm{Al}_7$ displays a field-induced magnetic transition for fields applied along the easy [001] direction at low temperatures, as indicated by magnetization measurements up to 14 T (upper panel in Fig. 11). A magnetization jump

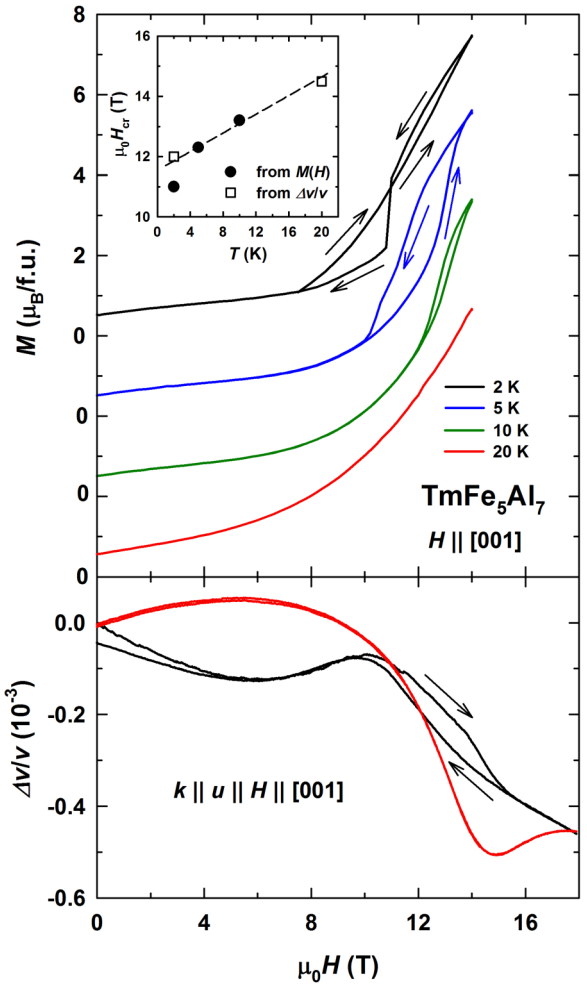

FIG. 11. (Color online) Magnetization (upper panel) and relative sound velocity change (lower panel) as a function of magnetic field applied along the [001] axis of $TmFe_5Al_7$ between 2 and 20 K. The inset shows the temperature dependence of the critical field of the field-induced transition determined from magnetization and acoustic measurements.

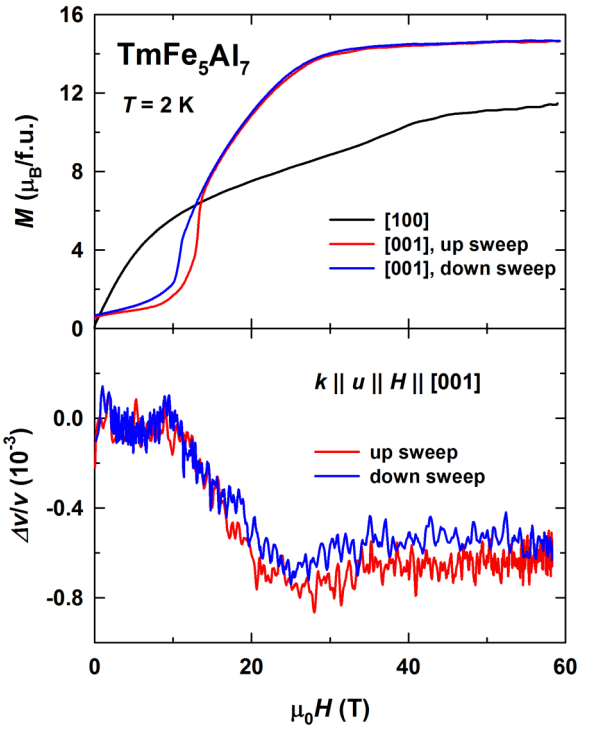

FIG. 12. (Color online) Magnetization (upper panel) and relative sound velocity change (lower panel) in pulsed magnetic fields up to 60 T applied along the [100] and [001] axes of $TmFe_5Al_7$ at 2 K.

is observed at 2 K with a complicated fine structure. The transition exhibits hysteresis and is of first order. A field of 14 T is not sufficiently high to register the full transition at this temperature. Up to this field, the compound is in a metastable state. This explains why at 11 T with decreasing field the magnetization drops below the values obtained with increasing field. At 5 and 10 K, the magnetization jump displays a smaller hysteresis, and a complete transition is seen in spite of the increasing critical field, H_{cr}. At $T = 20$ K, no transition is observed in the magnetization, although the positive curvature implies that a transition might exist above 14 T.

The change in the magnetic state at the magnetization jump modifies the electron-phonon coupling, which results in pronounced anomalies in acoustic properties. The relative change of the sound velocity measured up to 18 T at 2 K demonstrates a broad hysteresis at the transition that extends from 10 to 15 T (lower panel in Fig. 11). The transition at 20 K displays a negligible hysteresis. $\mu_0 H_{cr}$ at this temperature exceeds 14 T.

The inset in Fig. 11 shows the temperature dependence of the transition field determined from both the magnetization and acoustic properties as the average field between ascending and descending branches. The $\mu_0 H_{cr}$ value obtained from the magnetization at 2 K turns out to be too low. A more correct value is extracted from the $\Delta v/v$ dependence. Overall, H_{cr} increases linearly between 2 and 20 K where the transition is observed.

In order to observe all features of the complex magnetization process of $TmFe_5Al_7$, the magnetization was measured in pulsed magnetic fields up to 60 T (upper panel in Fig. 12). The magnetization for $\boldsymbol{H} \| [100]$ axis changes less fast around 10 T and displays a weak anomaly at about 37 T. At higher fields, the magnetization grows monotonously reaching 11.5 μ_B/f.u. at 60 T. This value is still far from the forced ferromagnetic state, $M_{ferro} = M_{Tm} + M_{Fe} = 14.5\ \mu_B$/f.u. The magnetization anomaly at 37 T should reflect the rotation of the Tm and Fe magnetic moments towards the [100] axis since this is the hard magnetization direction in this temperature range. The sound velocity and sound attenuation (not shown) were also measured along the [100] axis up to 60 T at 2 K. They did not show any anomaly. The anomaly in the magnetization disappears at 40 K.

Figure 12 also shows that a sharp stepwise anomaly occurs for $\boldsymbol{H} \| [001]$. The magnetization jump amounts to $\Delta M = 6\ \mu_B$/f.u. Below the magnetization jump, the Tm and Fe magnetic moments are almost antiparallel. The field-induced transition reflects the breaking of this alignment and stepwise rotation of the moments. Above the transition, the magnetization continues to grow as a function of field,

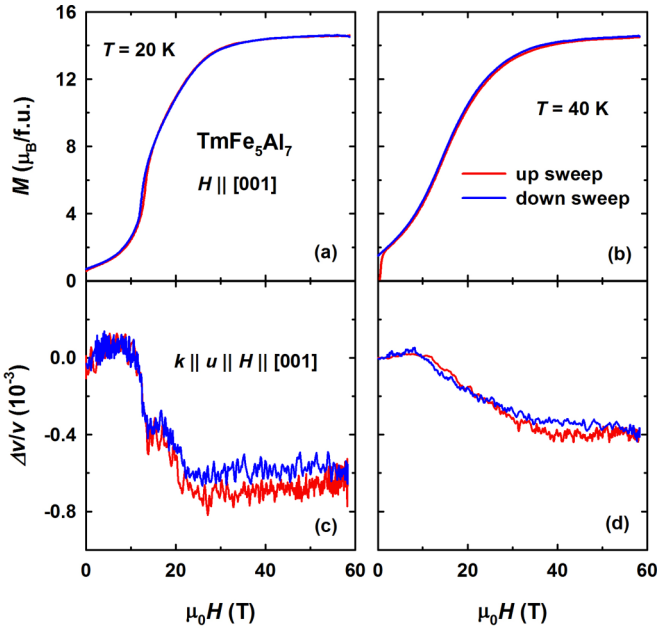

FIG. 13. (Color online) Magnetization (a), (b) and relative sound velocity change (c), (d) measured in pulsed magnetic fields up to 60 T along the [001] axis of $TmFe_5Al_7$ at 20 and 40 K.

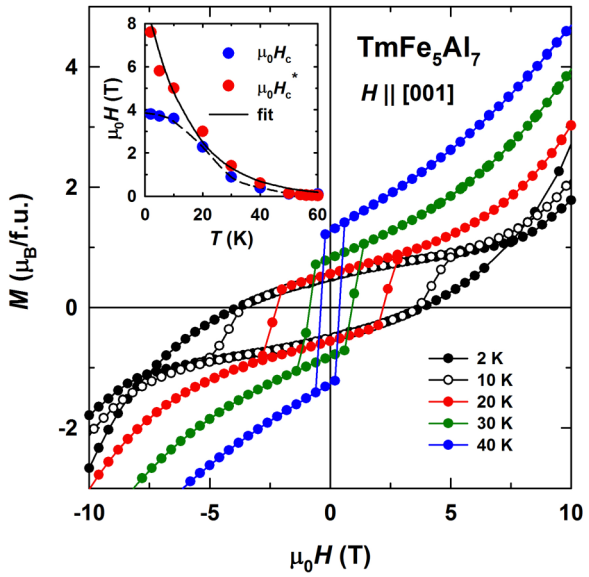

FIG. 14. (Color online) Hysteresis loops for $\boldsymbol{H}\|[001]$ of $TmFe_5Al_7$ between 2 and 40 K. The inset shows the temperature dependence of the coercivity, H_c, and loop half width, H_c^*. In the inset, the dashed line is a guide to the eye; the solid line is the fit $H_c^*(T) = 9.2\exp(-0.065T)$.

as the sublattice moments continue to rotate towards the minimum-energy direction. No other field-induced transitions are observed. The ferromagnetic saturation of 14.5 μ_B/f.u. is practically reached at about 30 T. The pronounced difference between the magnetization for $\boldsymbol{H}\|[100]$ and [001] points to a high magnetic anisotropy of the compound, whose uniaxial nature is related to the Tm sublattice.

Figure 12 also shows the relative sound velocity change of a longitudinal acoustic wave propagating along the [001] axis. The anomaly in $\Delta v/v$ is similar to that observed in static magnetic fields (see Fig. 11). At higher fields, the softening of the acoustic wave continues until the forced ferromagnetic state is reached.

The magnetization and acoustic properties measured for $\boldsymbol{H}\|[001]$ at 20 and 40 K are shown in Fig. 13. The field dependence of the magnetization at 20 K [Fig. 13(a)] is very similar to that at 2 K (see Figs. 11 and 12). In the sound velocity, a two-step anomaly appears close to the magnetization jump at about 14 T [Fig. 13(c)]. At higher fields in the saturated state, no more changes in $\Delta v/v$ are observed. At 40 K, the transition is smeared out and no longer seen in the magnetization [Fig. 13(b)]. $\Delta v/v$ displays a change in slope at about 10 T [Fig. 13(d)]. Typically, the acoustic properties are very sensitive to magnetic phase transitions, and one might assume that this feature reflects a stepwise rotation of the magnetic moments in $TmFe_5Al_7$. A similar situation was observed as well in the RFe_5Al_7 compounds with R = Tb, Ho, and Er: hardly any anomaly was seen in the magnetization, whereas the acoustic properties displayed pronounced anomalies [30–32]. However, the feature in $\Delta v/v$ of $TmFe_5Al_7$ at 40 K [Fig. 13(d)] has a shape different than at lower temperatures, without an abrupt decrease. Moreover, the transition field was found to increase with temperature (see inset in Fig. 11), which is not in line with the decrease in $\Delta v/v$ at about 10 T. From these considerations it follows that at 40 K the field-induced transition is no longer observed.

For completeness, we discuss the hysteresis due to domains in $TmFe_5Al_7$. Figure 14 shows hysteresis loops measured for $\boldsymbol{H}\|[001]$ between 2 and 40 K. $TmFe_5Al_7$, being an easy-axis ferrimagnet at these temperatures, displays strong magnetic hysteresis. The coercive field, $\mu_0 H_c$, is nearly 4 T at 2 K and rapidly falls off with increasing temperature (inset in Fig. 14). It should be noted that the loop shape is not rectangular due to the low magnetization and high susceptibility in a magnetic field. As a consequence, the $\mu_0 H_c$ values are much smaller than the loop half width, $\mu_0 H_c^*$, that reflects the field at which the magnetic hysteresis disappears completely. $\mu_0 H_c^*$ is just below 8 T at 2 K and decreases exponentially with temperature according to $H_c^*(T) = H_c^*(0)\exp(-\beta T)$, where $\mu_0 H_c^*(0) = 9.2$ T and $\beta = 0.065$ K^{-1}. Around 50 K, the loop half width is negligible. The strong magnetic hysteresis of the highly anisotropic ferrimagnet $TmFe_5Al_7$ with the strong temperature dependence may be related to a high intrinsic coercivity of narrow domain walls [40].

IV. CONCLUSIONS

The magnetization and magnetoacoustic properties of the ferrimagnet $TmFe_5Al_7$ ($T_C = 193$ K) have been studied in steady and pulsed magnetic fields up to 60 T. With increasing temperature, due to the competition between the uniaxial Tm anisotropy and planar Fe anisotropy, the compound displays a first-order spin-reorientation transition at 64 K from the [001] direction to the basal plane. The transition results in the appearance of a noncollinear magnetic structure

and a weakening of the intersublattice Tm-Fe exchange interaction. Under these circumstances, $TmFe_5Al_7$ undergoes a ferrimagnetic-antiferromagnetic phase transition. The antiferromagnetic structure is stable up to 82 K when it changes back to ferrimagnetic.

At low temperatures, field-induced phase transitions have been observed for fields applied along the easy [001] axis of $TmFe_5Al_7$. The anomalies reflect a stepwise rotation of the Tm and Fe magnetic moments before the forced ferromagnetic state is reached. Strong magnetoelastic interactions have been found at these magnetization jumps by use of sound-propagation measurements. Along the hard [100] direction, field-induced phase transitions have also been observed that reflect a discontinuous rotation towards this direction.

ACKNOWLEDGMENTS

The single-crystal growth and magnetization measurements in static magnetic fields were performed at the Magnetism and Low-Temperature Laboratories (MLTL, http://mltl.eu) supported within the Program of Czech Research Infrastructures (Project No. LM2011025). The work has been supported by the Czech Science Foundation (Grant No. 204/12/0150), the Czech Academy of Sciences (Grant No. M100101203), the Russian Foundation for Basic Research (Grant No. 12-02-00864) and Program UB RAS (Project No. 12-P2-1041). We acknowledge the support of HLD at HZDR, a member of the European Magnetic Field Laboratory (EMFL). D.I.G. acknowledges Charles University Grants No. SVV-2014-260091 and No. GAUK-703912.

[1] K. H. J. Buschow, in *Handbook of Magnetic Materials*, edited by E. P. Wohlfarth and K. H. J. Buschow (Elsevier, Amsterdam, 1988), Vol. 4, p. 1.

[2] M. D. Kuz'min and A. M. Tishin, in *Handbook of Magnetic Materials*, edited by K. H. J. Buschow (Elsevier, Amsterdam, 2008), Vol. 17, p. 149.

[3] B.-P. Hu, H.-S. Li, J. M. D. Coey, and J. P. Gavigan, Phys. Rev. B **41**, 2221 (1990).

[4] O. Moze, R. Caciuffo, Hong-Shuo Li, Bo-Ping Hu, J. M. D. Coey, R. Osborn, and A. D. Taylor, Phys. Rev. B **42**, 1940 (1990).

[5] X. C. Kou, T. S. Zhao, R. Grössinger, and F. R. de Boer, Phys. Rev. B **46**, 6225 (1992).

[6] X. C. Kou, T. S. Zhao, R. Grössinger, H. R. Kirchmayr, X. Li, and F. R. de Boer, Phys. Rev. B **46**, 11204(R) (1992).

[7] B.-P. Hu, K.-Y. Wang, Y.-Z. Wang, Z.-X. Wang, Q.-W. Yan, P.-L. Zhang, and X.-D. Sun, Phys. Rev. B **51**, 2905 (1995).

[8] Z.-h. Cheng, B.-g. Shen, Q.-w. Yan, H.-q. Guo, D.-f. Chen, C. Gou, K. Sun, F. R. de Boer, and K. H. J. Buschow, Phys. Rev. B **57**, 14299 (1998).

[9] N. P. Duong, E. Brück, P. E. Brommer, A. de Visser, F. R. de Boer, and K. H. J. Buschow, Phys. Rev. B **65**, 020408(R) (2001).

[10] N. Plugaru, J. Rubín, J. Bartolomé, C. Piquer, and M. Artigas, Phys. Rev. B **65**, 134419 (2002).

[11] J. L. Wang, B. García-Landa, C. Marquina, M. R. Ibarra, F. M. Yang, and G. H. Wu, Phys. Rev. B **67**, 014417 (2003).

[12] C. Piquer, J. Bartolomé, C. deFrancisco, and J. M. Muñoz, Phys. Rev. B **79**, 174430 (2009).

[13] W. Suski, in *Handbook on the Physics and Chemistry of Rare Earths*, edited by K. A. Gschneidner, Jr. and L. Eyring (Elsevier, Amsterdam, 1996), Vol. 22, p. 143.

[14] I. Felner, I. Nowik, and M. Seh, J. Magn. Magn. Mater. **38**, 172 (1983).

[15] I. Felner, I. Nowik, K. Baberschke, and G. J. Nieuwenhuys, Solid State Commun. **44**, 691 (1982).

[16] W. Kockelmann, W. Schäfer, G. Will, P. Fischer, and J. Gal, J. Alloys Compd. **207–208**, 311 (1994).

[17] D. I. Gorbunov, A. V. Andreev, and N. V. Mushnikov, J. Alloys Compd. **514**, 120 (2012).

[18] D. I. Gorbunov and A. V. Andreev, Solid State Phenom. **194**, 54 (2013).

[19] D. I. Gorbunov and A. V. Andreev, J. Alloys Compd. **556**, 109 (2013).

[20] D. I. Gorbunov and A. V. Andreev, J. Alloys Compd. **577**, 203 (2013).

[21] D. I. Gorbunov, A. V. Andreev, and M. D. Kuz'min, Phys. Rev. B **86**, 024407 (2012).

[22] D. I. Gorbunov, A. V. Andreev, S. Daniš, and J. Pospíšil, J. Alloys Compd. **563**, 63 (2013).

[23] D. I. Gorbunov, A. V. Andreev, and M. D. Kuz'min, J. Korean Phys. Soc. **62**, 1517 (2013).

[24] X. C. Kou, T. S. Zhao, R. Grössinger, H. R. Kirchmayr, X. Li, and F. R. de Boer, Phys. Rev. B **47**, 3231 (1993).

[25] X. C. Kou, R. Grössinger, G. Wiesinger, J. P. Liu, F. R. de Boer, I. Kleinschroth, and H. Kronmüller, Phys. Rev. B **51**, 8254 (1995).

[26] A. V. Andreev, A. N. Bogatkin, N. V. Kudrevatykh, S. S. Sigaev, and Ye. N. Tarasov, Phys. Met. Metallogr. **68**(1), 68 (1989).

[27] J. P. Liu, F. R. de Boer, P. F. de Châtel, R. Coehoorn, and K. H. J. Buschow, J. Magn. Magn. Mater. **132**, 159 (1994).

[28] A. K. Zvezdin, in *Handbook of Magnetic Materials*, edited by K. H. J. Buschow (Elsevier, Amsterdam, 1995), Vol. 9, p. 405.

[29] D. I. Gorbunov, A. V. Andreev, Y. Skourski, and M. D. Kuz'min, J. Alloys Compd. **553**, 358 (2013).

[30] D. I. Gorbunov, S. Yasin, A. V. Andreev, Y. Skourski, Z. Arnold, S. Zherlitsyn, and J. Wosnitza, J. Phys.: Condens. Matter **26**, 136001 (2014).

[31] D. I. Gorbunov, S. Yasin, A. V. Andreev, Y. Skourski, S. Zherlitsyn, and J. Wosnitza, J. Magn. Magn. Mater. **357**, 61 (2014).

[32] D. I. Gorbunov, S. Yasin, A. V. Andreev, N. V. Mushnikov, Y. Skourski, S. Zherlitsyn, and J. Wosnitza, J. Magn. Magn. Mater. **365**, 56 (2014).

[33] A. V. Andreev, M. D. Kuz'min, Y. Narumi, Y. Skourski, N. V. Kudrevatykh, K. Kindo, F. R. de Boer, and J. Wosnitza, Phys. Rev. B **81**, 134429 (2010).

[34] O. Isnard, A. V. Andreev, M. D. Kuz'min, Y. Skourski, D. I. Gorbunov, J. Wosnitza, N. V. Kudrevatykh, A. Iwasa, A. Kondo, A. Matsuo, and K. Kindo, Phys. Rev. B **88**, 174406 (2013).

[35] Y. Skourski, M. D. Kuz'min, K. P. Skokov, A. V. Andreev, and J. Wosnitza, Phys. Rev. B **83**, 214420 (2011).
[36] B. Lüthi, *Physical Acoustics in the Solid State* (Springer, Heidelberg, 2007), p. 1.
[37] B. Wolf, B. Lüthi, S. Schmidt, H. Schwenk, M. Sieling, S. Zherlitsyn, and I. Kouroudis, Physica B **294–295**, 612 (2001).
[38] A. V. Andreev, Physica B **404**, 2978 (2009).
[39] A. S. Ermolenko, E. V. Rozenfel'd, Yu. P. Irkhin, V. V. Kelarev, A. F. Rozhda, S. K. Sidorov, A. N. Pirogov, and A. P. Vokhmyanin, Zh. Eksp. Teor. Fiz. **69**, 1743 (1975) [Sov. Phys. JETP **42**, 885 (1975)].
[40] H. R. Hilzinger and H. Kronmüller, Phys. Status Solidi B **54**, 593 (1972).